

Photoelectrochemical Studies of Nanocrystalline TiO₂ Film Electrodes

Myung Soon Lee, Ik Chan Cheon, and Yeong Il Kim*

Department of Chemistry, Pukyong National University, Busan 608-737, Korea

Received April 1, 2003

Nanocrystalline semiconductor film electrodes have been prepared by sintering three different sizes of TiO₂ nanoparticle sols on conducting indium-tin-oxide (ITO) glass substrate. The electrochemical and photoelectrochemical properties of the prepared electrodes were comparatively investigated. The particle sizes, surface morphologies and crystallinities of the films were studied by scanning electron microscopy, transmission electron microscopy, and X-ray diffraction. Cyclic voltammetry and capacitance measurements in the dark implies the formation of depletion layer in the semiconductor films which was usually neglected in the previous studies and shows that flat band potential (E_{fb}) of TiO₂ films depends on the size of the composing particles. The band gap excitation of the film electrodes in aqueous electrolyte solution generated the anodic photocurrents from the oxidation of water. The photocurrent quantum yield of these TiO₂ films at the wavelength where all photocurrents are saturated increased as the particle size decreased. The photopotential measurements show that band edges of all three electrodes herein investigated were unpinned and shifted anodically under illumination. The pH dependence on band edge shift under illumination was different from that, which followed normal Helmholtz potential shift, in the dark.

Key Words : Nanocrystalline, TiO₂, Photoelectrochemistry, Photopotential, Nanoparticle

Introduction

Nanocrystalline semiconductor film electrodes have recently become a central research topic in the field of photoelectrochemistry, following the introduction of the dye-sensitized nanocrystalline semiconductor solar cell by Grätzel *et al.*^{1,2} "Grätzel's cell" exhibited almost 100% quantum efficiency in a certain wavelength range and about 10% solar conversion efficiency. As with photoelectrochemical solar cells, nanocrystalline semiconductor film electrodes also have shown the possibility of wide practical applications in such as electrochromic devices,³ batteries⁴ and photocatalysis.⁵ The film is composed of a three-dimensional network of interconnected nano-sized particles and has huge internal surface area. It exhibits novel optical and electrical properties compared with that of bulk semiconductor. The charge separation and charge transport process in this electrode have been explained differently from that of normal bulk semiconductor electrode. In normal semiconductor electrode, a space charge layer forms at the interface of the semiconductor and electrolyte solution and charge carrier separation occurs as a result of the internal electric field formed at the depletion layer. However, in a nanocrystalline semiconductor electrode the interfacial kinetics have been considered more important than the internal electric field because the individual particles seem to be too small to form a depletion layer. The charge separation of photoexcited electron-hole pairs has been considered dominated by diffusion rather than by migration in the potential difference of the depletion layer.⁶

Although numerous studies have been published on these nanocrystalline semiconductor electrodes, most of them are devoted to the dye-sensitized systems. Not many were found for direct band-gap excitation. To understand the nanocrystalline electrode system further in its fundamental aspects, we prepared the nanocrystalline TiO₂ film electrodes that consisted of different sizes of nanoparticle TiO₂ and studied their electrochemical and photoelectrochemical properties in water oxidation by band-gap excitation, comparatively.

Experimental Section

Materials. Degussa P25 TiO₂ was purchased from Sanghyun Industry (Seoul, Korea). Titanium(IV) isopropoxide (97%), acetylacetone (99+%) and Triton X-100 were obtained from Aldrich. ITO glass (40 Ω /cm²) was purchased from Delta Technology (MN, USA). Acetonitrile was distilled with P₂O₅ before use. All other chemicals and solvents were reagent grade and used as received. Distilled water was deionized to resistivity 18 M Ω cm with a Barnstead Nanopure D4700 deionization system.

Preparation of Nanocrystalline Electrodes. Three different types of the nanocrystalline TiO₂ film were prepared. The first electrode was prepared with Degussa P25 TiO₂. Our method mainly followed that of Nazeeruddin *et al.*'s.^{1j} 0.3 g of TiO₂ (Degussa P25) was ground in a mortar with 1 mL of water and 0.1 mL of acetylacetone. After the powder was well dispersed, 4 mL of water and 0.05 mL of Triton X-100 were slowly added to give a colloidal sol. The colloidal sol was dropped on ITO glass and spread with a glass rod by sliding over the tape-covered edges of the ITO. After being dried in air for 30 min, the film was sintered at 420-450 °C

*To whom correspondence should be addressed. e-mail: ykim@pknu.ac.kr

for 2 hours. This TiO₂ electrode is denoted as TD electrode. The second electrode was prepared with TiO₂ sol which was made from the hydrolysis of titanium(IV) isopropoxide. The colloidal sol was prepared by a method similar to that of O'Regan *et al.*^{1c}: 2.5 mL of titanium(IV) isopropoxide and 0.4 mL of isopropanol were slowly dropped in 15 mL of water as the combination was vigorously stirred under nitrogen. After the addition was finished, 0.106 mL of 70% HNO₃ was added to the mixture and refluxed at about 85 °C for 8 hours. This TiO₂ sol was spin-coated on ITO glass at 3000 rpm. The TiO₂-coated ITO was heated at 420 °C for 10 min. This spin coating and heating were repeated totally three times and the TiO₂ film on ITO was finally annealed at 450 °C for 2 hours. The second electrode is denoted as TS electrode. For the third electrode, the colloidal sol that was used for TS electrode was autoclaved at 200 °C for 12 hours. The sedimentation occurred during autoclaving. The sol and precipitates were ground together in a mortar with 0.1 mL of acetylacetone, 4 mL of water and 0.05 mL of Triton X-100 until the well-dispersed colloidal sol formed. This autoclaved sol was cast on ITO glass and annealed to prepare the third electrode (TA) in the same way as TD electrode. The average amounts of TiO₂ films on ITO substrate were 6.9×10^{-4} , 2.0×10^{-4} and 1.4×10^{-4} g/cm² for TD, TA and TS film, respectively. The geometrical area of the electrodes exposed to the electrolyte solution was 1.5 cm².

Apparatus. All electrochemical measurements were done in a standard three-electrode cell by EG&G PAR 263A potentiostat. Pt counter, SCE reference electrode and KCl electrolyte were used for the measurement in an aqueous solution. The pH of electrolyte solution was adjusted with 0.1 M KOH and HCl solutions. For nonaqueous solution, a quasi-silver reference electrode and tetraethylammonium perchlorate (TEAP) electrolyte were used and the measured potential was calibrated from the potential of ferrocene. Photocurrent measurements were performed in a three-electrode cell that had a flat quartz window, using PAR 263A potentiostat and 300W Xe arc lamp made by ILC Technology as light source. The cell was equipped with 10 cm water filter and appropriate optical filters. To discriminate dark current, the optical chopper of Scitec Instruments was used. The light intensity was measured with a Moletron PM 10 power meter probe. Spectroelectrochemical experiments were performed with a Varian Cary 1 spectrophotometer and PAR 263A potentiostat. Photocurrent action spectra were measured with an SLM Aminco AB2 luminescence spectrometer and an PAR 263A potentiostat. The capacitance measurements for the Mott-Schottky plot were done with an PAR 263A potentiostat and Stanford S830 digital lock-in-amplifier. Transmission electron micrographs (TEM) of the colloidal sols were taken with a Jeol JFM 2000fxII transmission electron microscope and scanning electron micrographs (SEM) of nanocrystalline TiO₂ film electrodes were taken with a Hitachi U-4200 scanning electron microscope. X-ray diffraction patterns (XRD) were measured by a Rigaku D/Max-200 X-ray diffractometer with a CuK α source and 0.01°/sec scan rate.

Results and Discussion

Characteristics of Nanocrystalline TiO₂ Films. Figure 1 shows the TEM pictures of TiO₂ nanoparticle sols that were used to prepare nanocrystalline TiO₂ film electrodes. The particle sizes of the colloidal sol from Degussa P25 TiO₂ were between 10-35 nm in diameter. The average diameter was about 25 nm, which is similar to the value previously reported.⁷ The TiO₂ particles that were prepared from the hydrolysis of titanium(IV) isopropoxide for TS electrode ranged in diameter from 4-6 nm. The diameters of particles in the autoclaved sol for TA electrode ranged from 10-12 nm. Figure 2 shows SEM micrographs of the nanocrystalline TiO₂ films. From the pictures, we can see clearly the nanocrystalline characteristics of the TiO₂ films on ITO and

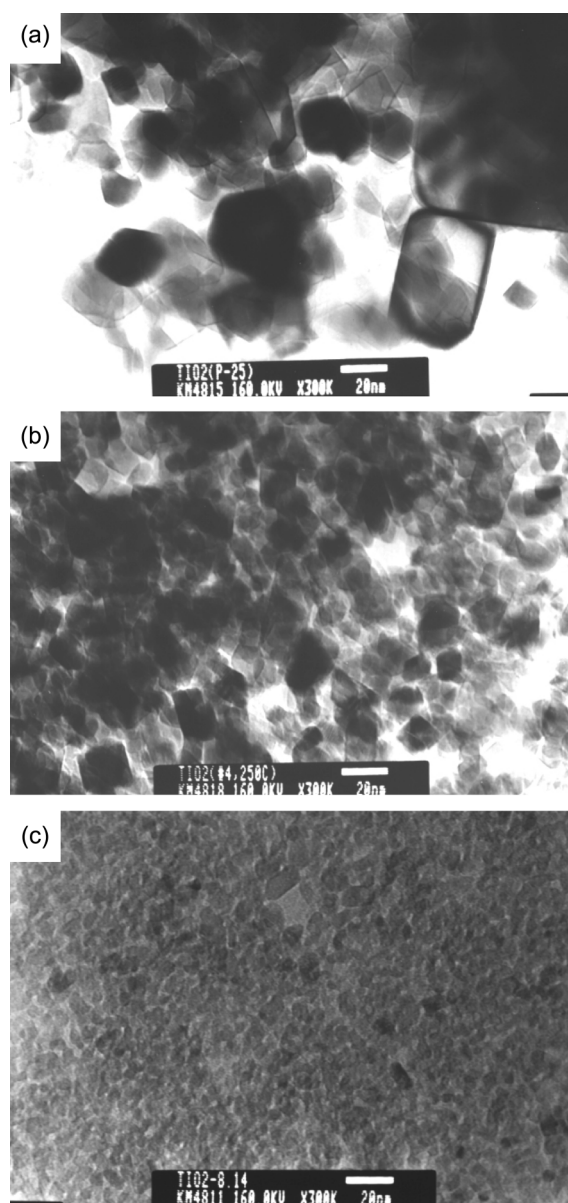


Figure 1. Transmission electron micrographs of the colloidal TiO₂ sols that are used for (a) TD, (b) TA and (c) TS electrodes. Scales and magnifications are indicated on the photographs.

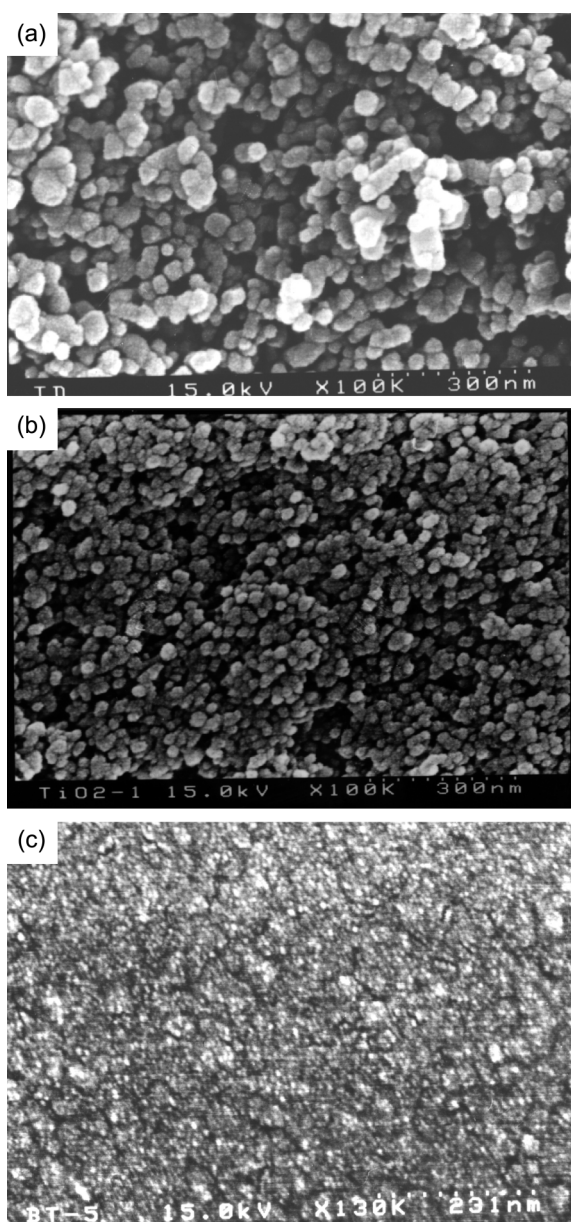


Figure 2. Scanning electron micrographs of the TiO₂ films of (a) TD, (b) TA and (c) TS electrode. Scales and magnifications are indicated on the photographs.

the porosity of the three films increases as the order of increasing size of composing particles. The particles composing the films were apparently larger than those of the corresponding colloidal sols. This could be due to the aggregation of particles during the annealing processes at 450 °C. The film of the TS electrode is most compact and dense, as shown in Fig. 2(c). The cross sectional views of these films in the SEM pictures (not shown here) led to an estimate of the thicknesses of the films of about 5 μm for TD, *ca.* 0.8 μm for TA and *ca.* 0.6 μm for TS film.

Figure 3 shows the XRD patterns of these three TiO₂ films. For TD film, the XRD pattern consists of the peaks corresponding to both crystal structures of anatase and rutile as indicated in Figure 3(a). From the peak intensity ratio of

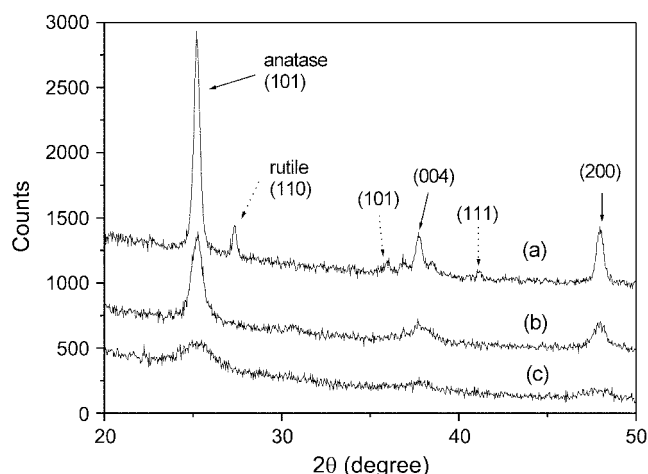


Figure 3. XRD patterns of the nanocrystalline TiO₂ films of (a) TD, (b) TA and (c) TS electrode.

anatase vs. rutile, it can be ascertained that the composition of TD film follows that of original Degussa P25 TiO₂, which is known to be approximately 25% rutile and 75% anatase. For TS and TA films only the anatase phase was observed in the XRD patterns (Figure 3b and 3c). From the line widths of XRD peak (anatase 101) of the films, we have also roughly estimated the particle sizes of TiO₂ in the films using the Debye-Scherrer equation⁸: 32.6 nm for TD, 21.7 nm for TA and 13.0 nm for TS. These results are consistent with those estimated from TEM pictures.

Figure 4 shows the absorption spectra of these nanocrystalline TiO₂ films, which are normalized by the absorbance at 250 nm. For TD film, the absorption was measured in diffuse reflectance mode since the film was not transparent enough for transmission mode. The absorption edges were blue-shifted as the particle sizes of the films decreased. The band gap energy of a semiconductor is generally determined by the following relationship between the absorption coefficient α and band gap energy E_g : $\alpha = (h\nu -$

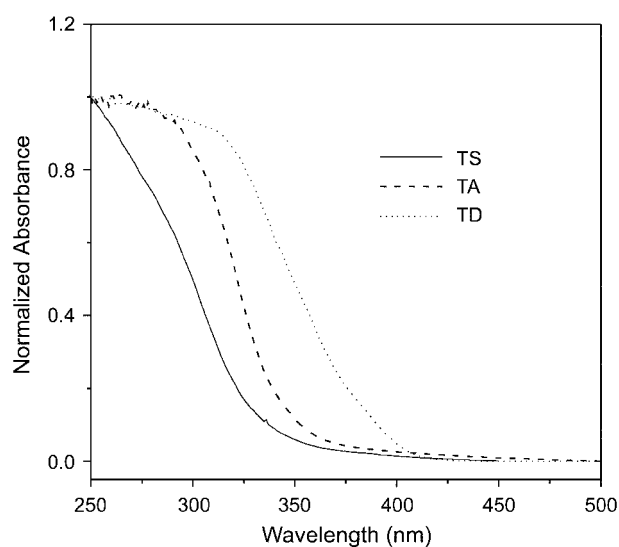


Figure 4. UV-Vis absorption spectra of TiO₂ films. (For the TD film the spectrum was measured at diffuse reflectance mode).

E_g^n , where $n = 1/2$ for direct band gap semiconductor and $n = 2$ for indirect band gap.⁹ Since TiO_2 is known to be an indirect band gap semiconductor,¹⁰ plots of the square root of absorbance vs. photon energy gave band gap energies roughly as 3.6, 3.4 and 3.1 eV for TS, TA and TD, respectively. The band gap energies of TiO_2 for TA and TS electrodes are slightly larger than the known value of anatase TiO_2 and that for TD electrode is close to the band gap energy of rutile TiO_2 .¹¹ The increased band gap energies for TA and TS films can be attributed to size quantization effect, although the interconnection between particles in the films makes the situation complicated. According to the calculation of the modified particle-in-a-sphere model for the size dependence of semiconductor band gaps,¹² the TiO_2 particle having a diameter of 2 nm demonstrated that the band gap energy increased as 0.2 eV compared with that of bulk TiO_2 . Therefore, the increased band gap energies for TA and TS electrodes (0.2-0.4 eV for the particles of 4-10 nm) are a little high to be entirely explained by size quantization effect. For the TD electrode of which TiO_2 particles are the largest in size, the determined band gap is mainly ascribed to the rutile particles therein rather than to anatase TiO_2 , which is a major component. This is because the absorption edge is determined by the species absorbing the longest wavelength.

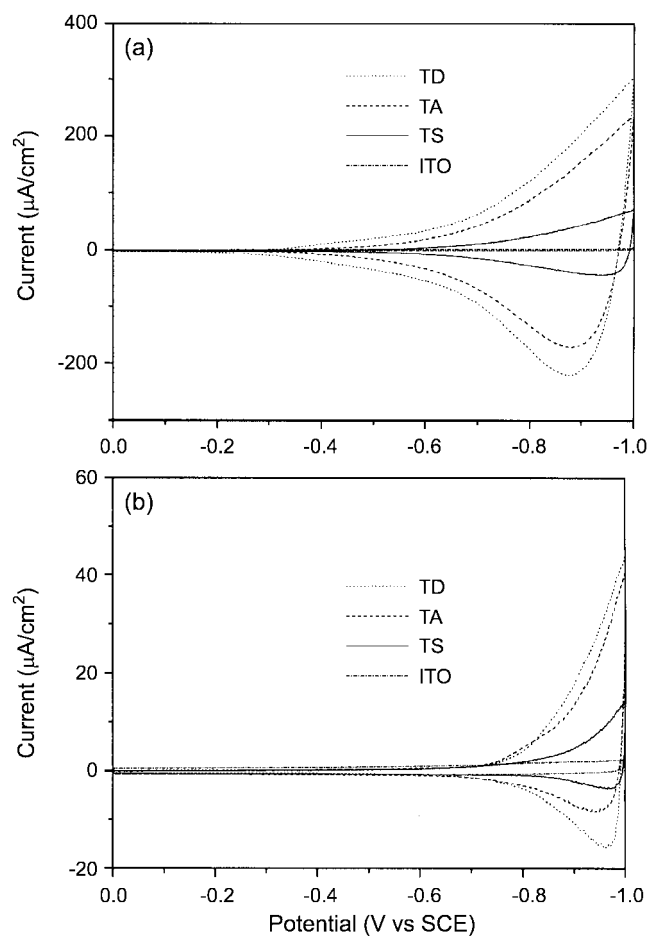


Figure 5. Cyclic voltammograms of the nanocrystalline TiO_2 film electrodes and ITO at (a) pH 6 and (b) pH 13 in 0.1 M KCl solution. (The scan rate is 25 mV/s)

In this particle size, there is no band gap increment observed.

Cyclic Voltammetry of Nanocrystalline TiO_2 Electrodes

Figure 5 shows cyclic voltammograms of the nanocrystalline TiO_2 and bare ITO electrodes in an aqueous KCl solution at pH 6 and 13. For all three TiO_2 film electrodes, the apparent reduction current appeared and increased steadily as the applied potential increased in the negative potential region. The oxidation current occurred as the potential sweep reversed, whereas such a current was not observed for the substrate ITO electrode. The onset potential of the reduction current varied at three different electrodes. The electrode that consisted of smaller TiO_2 particles showed more negative onset potential. The onset potential was also shifted to negative potential as the pH of electrolyte solution increased.

Since there is no faraday component in the electrolyte solution except solvent water, the observed current can be a charging current that is associated with several capacitance components or can be a reduction current of proton in the electrolyte solution. The cyclic voltammogram of a single crystal TiO_2 electrode in an aqueous electrolyte solution had a shape similar to that of the nanocrystalline TiO_2 electrode.¹³ The voltammogram was interpreted as consisting of a slowly increasing charging current that was proportional to the space charge capacitance and sharply increasing proton reduction current at potentials more negative than flat band potential (E_{fb}). However, the sharp increase in the reduction current for the nanocrystalline TiO_2 electrodes, as shown in Figure 5, cannot be simply attributed to the reduction of proton because the same voltammograms were obtained in nonaqueous aprotic solvents.¹⁴ Grätzel *et al.* also reported similar cyclic voltammograms of nanocrystalline TiO_2 electrodes in nonaqueous propylene carbonate.¹⁵⁻¹⁷ At first, they interpreted the smoothly increasing current as the capacitive charging current that is due to filling of the surface states below the conduction band edge and estimated the surface state density by simply integrating the charging current to a certain potential.¹⁵ Later, they reported the characteristic peak near the current onset in the voltammogram and the peak was attributed to filling of the surface states or resistance-induced effects. The voltammetric charge during negative scan was interpreted as two components that are the trapped charge in empty surface states and the accumulated charge in a space charge layer.¹⁶ In another report they interpreted the voltammogram as the capacitive effect associated with the formation of accumulation layer, which is related to the surface redox process, $\text{Ti}^{4+} + e^- \leftrightarrow \text{Ti}^{3+}$.¹⁷ The arguments of Grätzel *et al.* are not consistent and very controversial. On the other hand, according to the electrochemical quartz crystal microbalance studies by Hupp *et al.*,¹⁸ the cathodic current was interpreted as due to the charge compensating cation intercalation into the accumulation region in the semiconductor film.

In a normal n-doped semiconductor electrode the accumulation layer is formed at potentials more negative than a flat band potential, and the electrode become metallic.^{10,19} And the charging current will start at a flat band potential due to double layer capacitance, becoming constant at a constant

scan rate of potential. Contrary to a normal semiconductor electrode, the observed charging currents on the nanocrystalline TiO₂ electrodes were dependent on the applied potential. At this point the origin of the current in the voltammograms is not clear. It can be due to the complex capacitive components that consist of space charge capacitance, surface state capacitance and double layer capacitance as well as due to charge compensating cation intercalation. However, the current onset potential can be assigned to the flat band potential since the onset potential shows the clear pH-dependent shift roughly following the well-known Helmholtz potential shift ($-59 \text{ mV per } \Delta\text{pH } 1$) for a metal oxide semiconductor electrode.²⁰

Capacitance Characteristics of Nanocrystalline TiO₂ Electrodes. To elucidate the formation of space charge layer at the interface with electrolyte solution and determine the band edge position, we have measured the potential dependence of capacitance at the interface between the electrode and electrolyte solution under depletion condition. According to Mott-Schottky (M-S) equation, the differential capacitance of space charge layer is dependent on the applied potential as follows: $1/C^2 \propto E - E_{fb} - kT/e$, where C is the differential capacitance of the space-charge layer and E_{fb} is a flat band potential. Figure 6 shows the M-S plots for the nanocrystalline TiO₂ electrodes and a bare ITO electrode, measured at the frequency of 10 Hz and pH 6. While there was no dramatic change of capacitance for the bare ITO electrode as the bias potential increased to positive, all the TiO₂ film electrodes showed sudden increases in $1/C^2$ at certain potentials as the bias potential increased. In Figure 7, the pH dependence of M-S plots is shown. If we assume that the intercept potential is the flat band potential shown in M-S equation, the flat band potentials can be obtained from the linear fit of the data at three different pHs shown in Figure 6 and 7 as follows: $-0.18 - 0.043\text{pH}$, $-0.2 - 0.044\text{pH}$ and $-0.25 - 0.05\text{pH V vs. SCE}$ for TD, TA and TS electrode, respectively. Therefore, the potential was shifted to negative value systematically as the TiO₂ particle size composing the

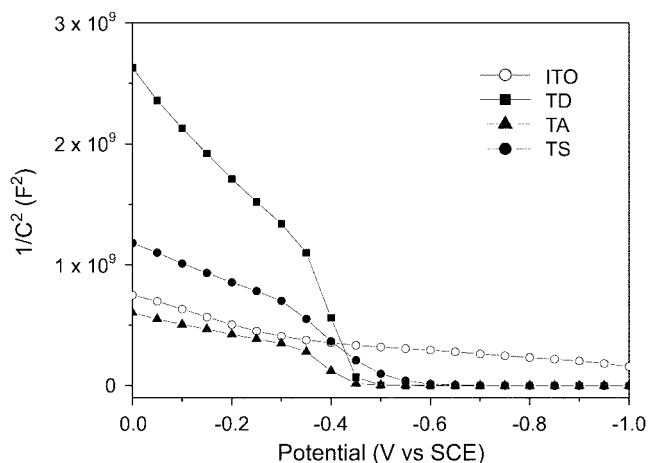


Figure 6. Mott-Schottky plots of the nanocrystalline TiO₂ film electrodes at 0.1 M KCl and pH 6 with the modulation frequency of 10 Hz.

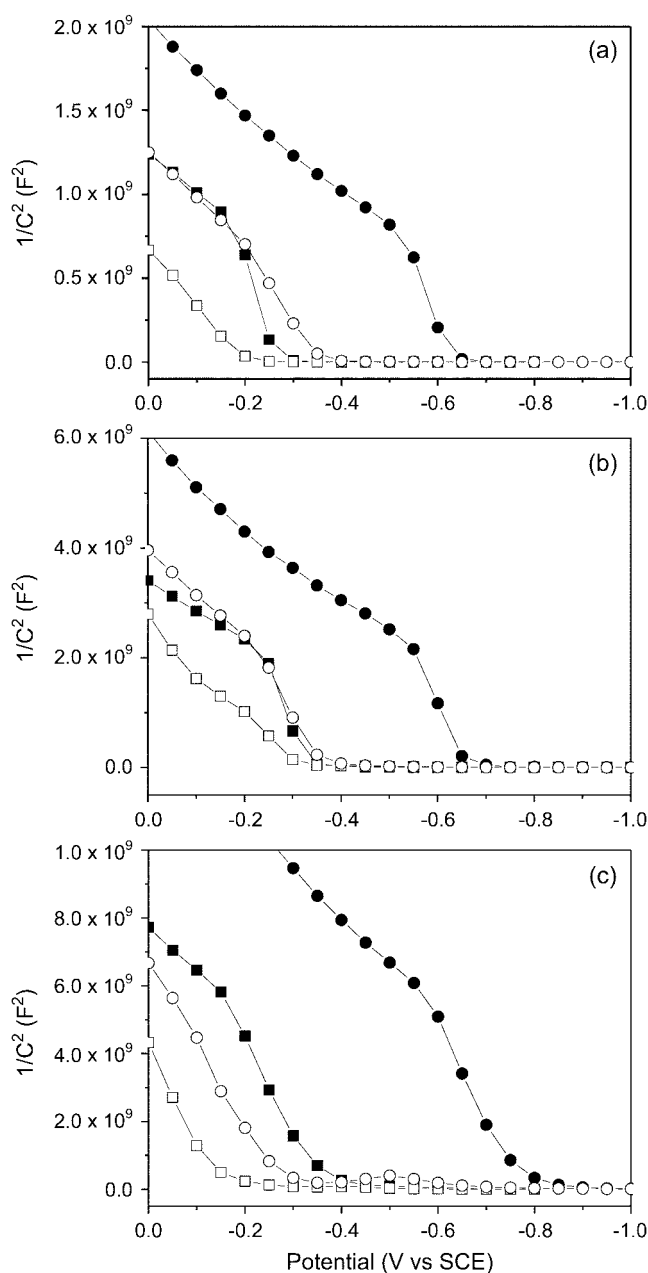


Figure 7. Mott-Schottky plots of the nanocrystalline TiO₂ film electrodes at pH 3 (squares) and pH 11 (circles) in dark (dark symbol) and under illumination (blank symbol): (a) TD, (b) TA and (c) TS electrode.

electrodes decreased and the pH dependence of E_{fb} followed roughly the potential shift of Helmholtz double layer. The estimated E_{fb} of the three electrodes shows somehow the difference from the reported value of the nanoporous TiO₂ film (similar to our TS electrode), which was estimated by spectroscopic measurement of conduction band electrons in the film: $-0.4 - 0.06\text{pH V vs SCE}$.²¹

Cao *et al.*²² studied the capacitance of a nanoporous TiO₂ film electrode that was almost the same as our TD electrode and showed that there was a large frequency dispersion in the Mott-Schottky plot for the electrode and the high potential dependence at high frequency was due to ITO

substrate and the low potential dependence at low frequency was due to TiO₂ film. They concluded that the capacitance of TiO₂ film measured at low frequency was independent of potential because the TiO₂ particles were fully depleted of electrons and behaved as a dielectric due to the small size. Hagfeldt *et al.* also asserted that the measured capacitance in a nanocrystalline TiO₂ electrode was dominated by the back contact of the conducting substrate rather than by TiO₂ film.²³ Although the Mott-Schottky plots obtained here were not as linear as expected in a bulk semiconductor electrode, there is an obvious potential dependence in the measured capacitances, as shown in Figure 6 and 7. Since TiO₂ particles of the nanocrystalline film electrodes were interconnected and partly fused together, we think that the all films can show some bulk properties of semiconductor rather than being completely dominated by the individual particles as Cao and Hagfeldt *et al.* assumed. In that case there is a possibility of the formation of a space charge layer in the film and the observed potential dependence of capacitance can be due to the space charge layer capacitance at least under the depletion condition, albeit the complexity exists under the accumulation condition.

Hagfeldt *et al.* also reported that a differential capacitance of a nanocrystalline TiO₂ film electrode was measured under band gap illumination and the conduction band edge was shifted positively, while the capacitance in the dark was dominated by the back contact substrate as mentioned above.²³ They interpreted that the shift of band edge was due to the trapping of photogenerated holes in midbandgap surface states leading to the unpinning of the energy band. We have also measured the capacitance of the nanocrystalline TiO₂ electrodes prepared here under band gap illumination. The M-S plots were shown as blank symbols in Figure 7. The onset potentials were shifted by about +0.4 V at pH 11 and about +0.2 V at pH 3 for TS electrode and about +0.3 V at pH 11 and +0.1 V at pH 3 for both TD and TA electrode, respectively. Thus, the pH dependence of the potential shift under band gap illumination became much smaller (about 13 mV/unit pH) than in the dark (about 40-50 mV/unit pH). This band edge unpinning under illumination could be due to the trapping of minority carriers in the surface states as Hagfeldt *et al.* interpreted. It is not primarily necessary, however, because the minority carriers can be accumulated at the surface by the internal electric field if the space charge layer is formed and leads to changes in the potential distribution. It is an interesting finding that the band edge shift under illumination did not follow the same pH dependence as in dark. At this point the reason is not clear and further investigation is needed.

Photocurrent Characteristics of Nanocrystalline TiO₂ Electrodes. TiO₂ electrodes have been known to generate photocurrents from water oxidation by generated holes under band gap illumination.²⁴ Figure 8 shows the photocurrent-potential characteristics of our nanocrystalline TiO₂ electrodes in 0.1 M KCl aqueous solution under white light illumination. The photocurrent onset potentials are roughly -1.2 and -0.7 V vs SCE at pH 13 and 3, respectively in all

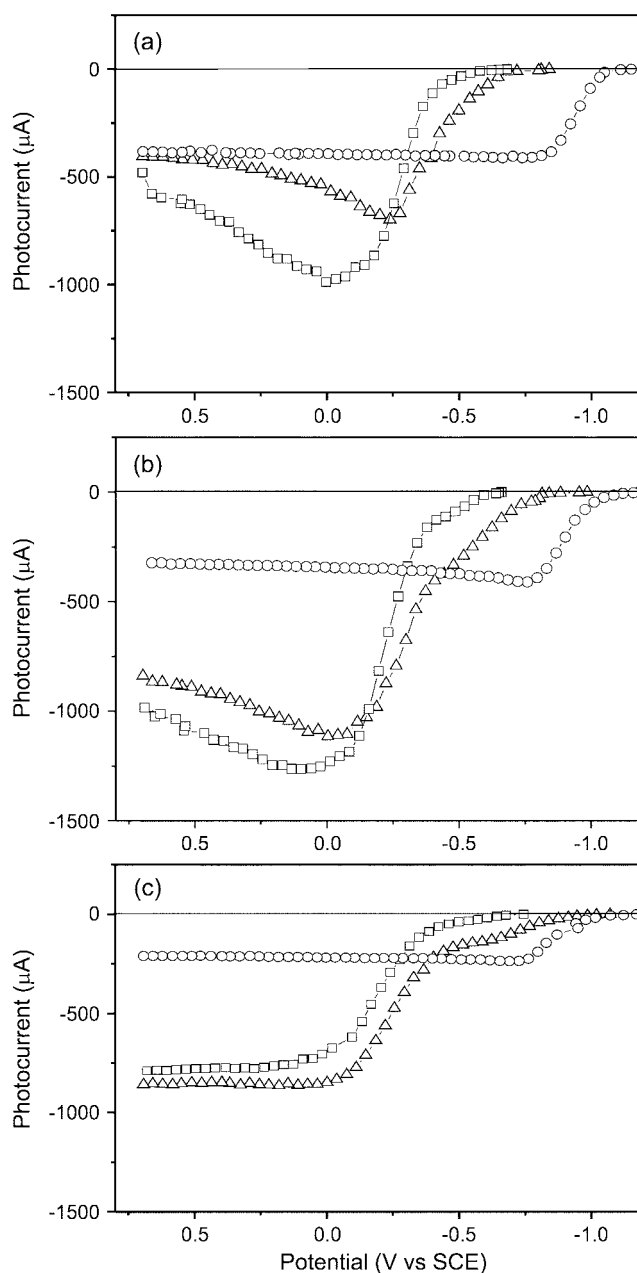


Figure 8. Photocurrent-potential characteristics of (a) TD, (b) TA and (c) TS electrode at pH 3 (□), 6 (△) and 13 (○) in 0.1 M KCl solution (light intensity: 346 mW/cm²).

three electrodes. These potentials are not coincident with the flat band potentials from M-S plots shown in Figure 6 and 7. The pH dependence of the onset potential follows the shift of Helmholtz potential as shown in M-S plots. The saturation photocurrents are larger at lower pH for the TD and TA electrode, whereas the neutral pH gave the largest photocurrent in the TS electrode. The larger photocurrents at lower pH can be understood by the more positive potential of photogenerated holes due to the Helmholtz potential shift. The decreases of the saturation photocurrents at more positive potentials for TD and TA electrodes were due to the time dependent decays of the photocurrents at those pHs. Figure 9 shows the time dependence of the photocurrents at

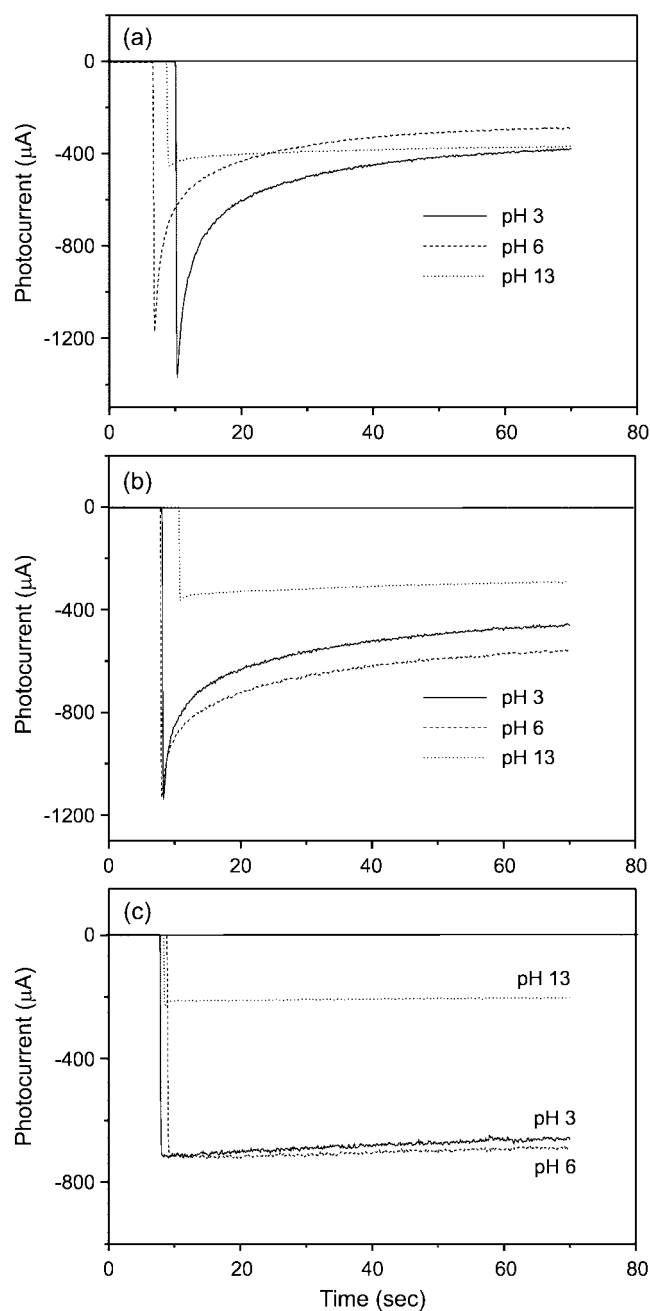


Figure 9. Time dependence of photocurrent of the nanocrystalline TiO₂ film electrodes at various pHs: (a) TD, (b) TA and (c) TS electrodes. (The potential was held at +0.5 V vs. SCE)

various pHs for the anodically biased three electrodes. For TA and TD electrodes, the current decays are serious at low pHs in the time scale of several tens of seconds, whereas the decays at TS electrode are not significant at all pHs measured here. The results show that the observed photocurrent decay at acidic condition also depends on the particle sizes of TiO₂ in the electrodes. The current decays cannot be attributed to the photocorrosion of TiO₂ since the electrodes showed the same results repeatedly when the electrode was reused after one experiment. And the anodic photocorrosion of TiO₂ was not known at all for even nanoparticles of TiO₂ as well as single crystal or polycrystalline TiO₂. This kind of

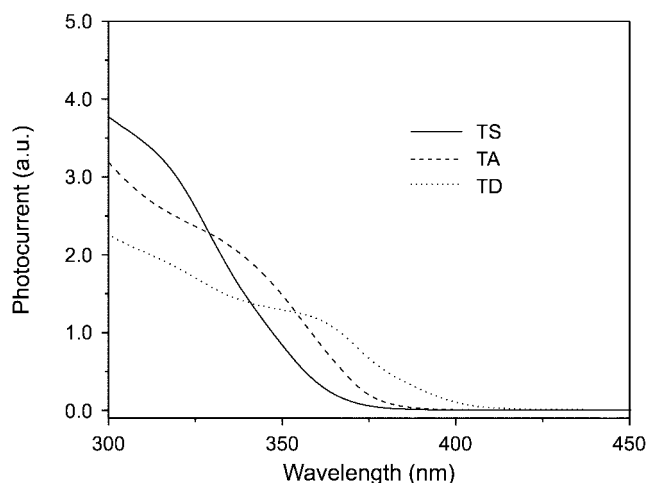


Figure 10. Photocurrent action spectra of the nanocrystalline TiO₂ film electrodes in 0.1M KCl, measured at 0.5 V vs. SCE.

photocurrent decays at other TiO₂ electrodes when the photocurrent was generated by water oxidation has not been reported so far as we know. Although the origin is not clear at this point, the decay may be related with the very slow trapping of photogenerated holes in surface defect sites of nanocrystalline TiO₂ particles.

The photocurrent action spectra of the TiO₂ film electrodes in the same illumination condition are shown in Figure 10. The current-onset wavelengths are consistent with the absorption edge wavelengths from the absorption spectra shown in Figure 4. Although the quantitative quantum yield was not calculated since the light intensity at each wavelength could not be measured, the relative comparison for the three electrodes is possible from the action spectra. At the wavelength where all the photocurrents are mostly saturated (<320 nm), the photocurrent quantum yield is the highest for TS electrode and the lowest for TD electrode. Since the thickness of the films in three types of electrodes is different, the difference of photocurrent efficiency between those electrodes may not be due to only the difference of the intensive characteristics of those films. However, we have prepared a few of electrodes with different thickness for each type of electrode and used the electrode herein with optimized results within the available range of thickness. Therefore, the difference of photocurrent efficiency can mostly be ascribed to the difference of the intensive properties of the films. There are two major factors that affect photocurrent efficiency: one is the different band gap energy due to different particle size, and the other is different density of surface states. The increased band gap will shift the oxidation potential of photo-generated holes positively and result in the increased photocurrent. This factor is easily rationalized since the electrode with a smaller particle size and larger band gap energy gave the larger photocurrent. In the second factor, the surface states are well known to play a role of charge trapping and charge recombination center and decrease photocurrent efficiency. Therefore, the difference of density of surface states between three types of films must

have contributed partly to the difference of photocurrent efficiency. Since the difference of the surface-state density between those electrodes could not be determined quantitatively, it is hard to tell which factor had the biggest effect on efficiency at this point.

Conclusions

We have prepared three different types of nanocrystalline TiO₂ film electrodes, which were consisted of three different sizes of composing particles, and studied their photoelectrochemical properties comparatively. The measured differential capacitance implies the formation of a space charge layer that was usually neglected in the studies of dye-sensitized nanocrystalline semiconductor electrodes. The flat band potentials determined from M-S plots shifted negatively as the particle sizes composing the film electrode decreased. The band gap excitation of the film electrodes in aqueous electrolyte solution yielded the anodic photocurrents due to the oxidation of water depending on pH of the electrolyte solution. The photocurrent action spectra shows that the photocurrent quantum yield at the wavelength where all photocurrents are saturated increases as the composing particle sizes decreases. The photocapacitance measurements shows that the band edges of all three electrodes herein investigated were unpinned and shifted anodically under illumination and the pH dependencies were different from that in the dark, which follows normal Helmholtz potential shift. The photocurrent decay in the time scale of several tens of seconds was observed and the decay rates were dependent on the composing particle sizes. To clarify the results presented here, further investigations are needed.

Acknowledgement. This work was supported by Non Directed Research Fund, from Korean Research Foundation, 1996 and 1997.

References

- (a) Desilvestro, J.; Grätzel, M.; Kavan, L.; Moser, J. *J. Am. Chem. Soc.* **1985**, *107*, 2988. (b) Vrachnou, E.; Vlachopoulos, N.; Grätzel, M. *J. Chem. Soc. Chem. Commun.* **1987**, 868. (c) Kalyanasundram, K.; Vlachopoulos, N.; Krishnan, V.; Monnier, A.; Grätzel, M. *J. Phys. Chem.* **1987**, *91*, 2342. (d) Vlachopoulos, N.; Liska, P.; Augustynski, J.; Grätzel, M. *J. Am. Chem. Soc.* **1988**, *110*, 1216. (e) O'Regan, B.; Moser, J.; Anderson, M.; Grätzel, M. *J. Phys. Chem.* **1990**, *94*, 8720. (f) Nazeeruddin, M. K.; Liska, P.; Moser, J.; Vlachopoulos, N.; Grätzel, M. *Helv. Chim. Acta* **1990**, *73*, 1788. (g) Frei, H.; Fitzmaurice, D. J.; Grätzel, M. *Langmuir* **1990**, *6*, 198. (h) O'Regan, B.; Grätzel, M. *Nature* **1991**, *353*, 737. (i) Kavan, L.; O'Regan, B.; Kay, A.; Grätzel, M. *J. Electroanal. Chem.* **1993**, *346*, 291. (j) Nazeeruddin, M. K.; Kay, A.; Rodicio, I.; Humphry-Baker, R.; Müller, E.; Liska, P.; Vlachopoulos, N.; Grätzel, M. *J. Am. Chem. Soc.* **1993**, *115*, 6382.
- (a) Sviridov, D. V.; Kulak, A. I. *New J. Chem.* **1991**, *15*, 539-544. (b) Amadelli, R.; Argazzi, R.; Bignozzi, C. A.; Scandola, F. *J. Am. Chem. Soc.* **1990**, *112*, 7099. (c) Murakoshi, K.; Kano, G.; Wada, Y.; Yanagida, S.; Miyazaki, H.; Matsumoto, M.; Murasawa, S. *J. Electroanal. Chem.* **1995**, *396*, 27. (d) Bae, J. H.; Kim, D.; Kim, Y. I.; Kim, K.-J. *Bull. Korean Chem. Soc.* **1997**, *18*, 567. (e) Park, N.-G.; Chang, S.-H.; Lagemaat, J.; Kim, K.-J.; Frank, A. *J. Bull. Korean Chem. Soc.* **2000**, *21*, 985. (f) Kang, M. G.; Park, N.-G.; Chang, S. H.; Choi, S. H.; Kim, K.-J. *Bull. Korean Chem. Soc.* **2002**, *23*, 140.
- Hagfeldt, A.; Vlachopoulos, N.; Grätzel, M. *J. Electrochem. Soc.* **1994**, *141*, L82.
- Huang, S.; Kavan, L.; Kay, A.; Grätzel, M. *J. Active Passive Electron. Comput.* **1995**, *18*, 23. (b) Huang, S.; Kavan, L.; Exnar, I.; Grätzel, M. *J. Electrochem. Soc.* **1995**, *142*, L142.
- Vinodgopal, K.; Hotchandani, S.; Kamat, P. V. *J. Phys. Chem.* **1993**, *97*, 9040.
- Hagfeldt, A.; Grätzel, M. *Chem. Rev.* **1995**, *95*, 49.
- Lindström, H.; Rensmo, H.; Södergren, S.; Solbrand, A.; Lindquist, S.-E. *J. Phys. Chem.* **1996**, *100*, 3084.
- Azaroff, L. B. *The Powder Method*; McGraw Hill: New York, 1958.
- Butler, M. A. *J. Appl. Phys.* **1977**, *48*, 1914.
- Koffyberg, F. P.; Dwight, K.; Wold, A. *Solid State Commun.* **1979**, *30*, 433.
- Finklea, H. O. *Semiconductor Electrodes*; Elsevier: New York, 1988; p 50.
- Kim, Y. I.; Keller, S. W.; Krueger, J. S.; Yonemoto, E. H.; Saupe, G. B.; Mallouk, T. E. *J. Phys. Chem. B* **1997**, *101*, 2491.
- Reference 11, p 81.
- We have obtained a similar voltammogram with the almost same current scale in a dry acetonitrile solution of 0.1 M TEAP.
- Kay, A.; Humphry-Baker, R.; Grätzel, M. *J. Phys. Chem.* **1994**, *98*, 952.
- Kavan, L.; Kratochvilova, K.; Grätzel, M. *J. Electroanal. Chem.* **1995**, *394*, 93.
- Kavan, L.; Grätzel, M.; Rathousky, J.; Zúkal, A. *J. Electrochem. Soc.* **1996**, *143*, 394.
- (a) Lyon, L. A.; Hupp, J. T. *J. Phys. Chem.* **1995**, *99*, 15718. (b) Lemon, B. I.; Hupp, J. T. *J. Phys. Chem.* **1996**, *100*, 14578. (c) Lemon, B. I.; Hupp, J. T. *J. Phys. Chem.* **1997**, *101*, 2426.
- Reference 11, p 15.
- Morrison, S. R. *Electrochemistry at Semiconductor and Oxidized Metal Electrodes*; Plenum: New York, 1980; p 62.
- Rothenberger, G.; Fitzmaurice, D.; Grätzel, M. *J. Phys. Chem.* **1992**, *96*, 5983.
- Cao, F.; Oskam, G.; Searson, P. C.; Stipkala, J. M.; Heimer, T. A.; Farzad, F.; Meyer, G. J. *J. Phys. Chem.* **1995**, *99*, 11974.
- Hagfeldt, A.; Björkstén, U.; Grätzel, M. *J. Phys. Chem.* **1996**, *100*, 8045.
- Desplat, J.-L. *J. Appl. Phys.* **1976**, *47*, 5102.